Four-Headed Arrow Shaped Dual Band Perfect Absorbers for Biosensing Applications

Aytac Onur*[1], Mustafa Turkmen [1], Sabri Kaya [1]

Abstract: In this study, a novel perfect absorber (PA) array based on four-headed arrow nanoparticles for biosensing applications in mid-infrared regime is presented. Proposed PA array has a dual-band spectral response, and the locations of resonances can be adjusted by varying the geometrical dimensions of the structure. Nearly unity absorbance is obtained from the PA array for both resonances. Different dielectric spacers (MgF_2, SiO_2, and Al_2O_3) are used to investigate the effects of dielectric spacer on the absorbance characteristics of proposed PA array. Absorbance characteristics of PA array are analyzed by using finite difference time domain (FDTD) method. High field enhancement is achieved by the interaction of the sharp corners of arrow nanoparticles. Linear correlation between the resonance frequencies and the refractive index of cladding mediums is determined. Due to the high refractive index sensitivity and near-field enhancement, and nearly unity absorbance, the proposed dual-band PA array with adjustable spectral responses can be useful for biosensing applications in mid-infrared regime.

Keywords: Perfect absorber, Plasmonics, Biosensing applications

1. Introduction

A new research area of plasmonic structure is getting attention, known as plasmonic perfect absorbers (PAs) [1–6]. The concept of metamaterial PAs came from microwave regime, due to the advancement in the nanotechnology; it can be scaled down to the terahertz regime [7, 8]. The possibility of perfect absorption is revealed by appropriately engineering the electric and magnetic response of the incident field in gigahertz regime [7, 8]. The PAs are composed of periodically arranged resonant metallic nanoparticles and thin metal layer separated by a dielectric spacer [2, 5, 9]. There are many advantages of this kind of structures which include high absorptivity, small thickness, and low density [10]. With this type of device configuration, wide-angle, wide-band, and polarization-insensitive high absorption near unity can be achieved by matching the impedance of metamaterial absorbers to free space or with microcavity, hole arrays, and metallic surfaces [5, 9-11]. PAs operating in the infrared and visible regions have been used for biomedical sensing, surface-enhanced spectroscopy, and near-field scanning optical microscopy applications [1-15].

In this study, a four-headed arrow nanoparticle shaped PA array for biosensing applications in mid-infrared regime is presented. The optical properties of plasmonic PA array are investigated by using the finite difference time domain (FDTD) method [16]. In order to understand the physical origin of the resonant behavior and determine the field enhancement of the nanostructure, near field distributions at the resonant frequencies are obtained. Due to dual band spectral response and enhanced near field distribution, the proposed PA array can be useful for biosensing applications in mid-infrared regime.

2. Numerical analysis

Schematic view of proposed PA is illustrated in the Fig. 1(a). It consists of a dielectric spacer layer between nanoparticle-based top layer and gold (Au) film on a dielectric substrate (Si). Dielectric substrate thickness is 500 nm, gold film thickness is 200 nm, dielectric spacer layer thickness is 125 nm and four-headed arrow shaped gold nanoparticle thickness is 50 nm. In Fig.1 (a), L and d indicate the length and width of rectangular nanorods, respectively. h_1 indicates the heights of left and right triangular nanoparticles and h_2 indicates the heights of top and bottom triangular nanoparticles. w_1 indicates the base-widths of left and right triangular nanoparticles and w_2 indicates the base-widths of top and bottom triangular nanoparticles. Periodicities, Px and Py, of the array are 2000 nm. During the simulations, the analyses are performed under y-polarization illumination source and geometrical dimensions are chosen as L = 1000 nm, w_1 = 750 nm, w_2 = 700 nm, h_1 = 400 nm, h_2 = 350 nm, and d = 350 nm. Periodic boundary conditions are chosen as x- and y-axes, and perfectly matched layers are used along the z-axis. The dielectric constants of the materials are taken from Ref. [17].

Different dielectric spacers (MgF_2, SiO_2, and Al_2O_3) are used to investigate the effects of dielectric spacer on the absorbance characteristics of proposed PA array. The absorbance (A) spectra of the structure for different dielectric spacer (MgF_2, SiO_2, and Al_2O_3) are given in Fig. 1(b). It can be seen from Fig. 1(b), all structures exhibit dual-resonant behaviors in mid-IR regime. Also for all dielectric spacers, the absorption rates are nearly unity.

_____
[1] *Department of Electrical and Electronics Engineering,*
*ErciyesUniversity, 38100, Kayseri/Turkey*
* Corresponding Author:Email: aytac.onur@saglik.gov.tr
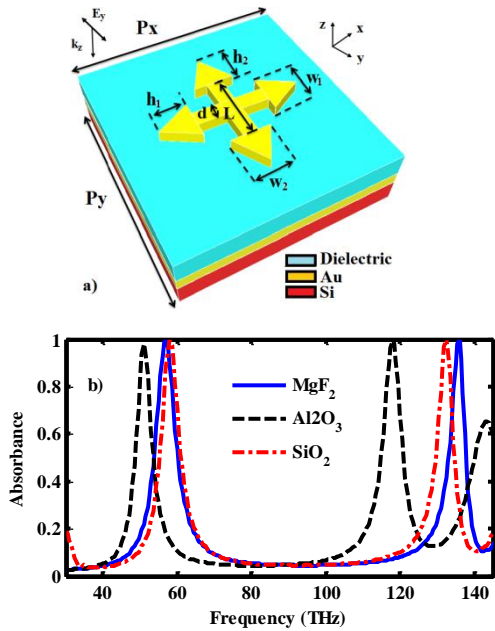
Fig. 1 (a) Schematic view of four-headed arrow shaped PA (b) Absorption spectra of four-headed arrow shaped PA for different spacer layers.

Figure 2(a) shows the absorbance (A), reflectance (R) and transmittance (T) spectra of the PA array with MgF_2 dielectric spacer. The absorbance spectra are calculated by $A = 1 - R - T$ [13]. Proposed PA has dual resonances and both of them rate as %99.9 at the first ($f_1 = 57$ THz) and at the second ($f_2 = 136$ THz) resonances. Electric field distributions are given in Figs. 2(b) and 2(c) at first (f_1) and second (f_2) resonances, respectively. The near field enhancements are greater than 2000 times are concentrated on the sharp corners of the structure. Molecules in these corners may undergo a much stronger interaction with the electromagnetic field than those that lie well away from metallic particles. This means that the dielectric environment of the near surface region of the proposed PA array can strongly influence the resonant frequencies. This phenomenon is the basis of the mid-infrared biosensing capabilities of proposed PA array.
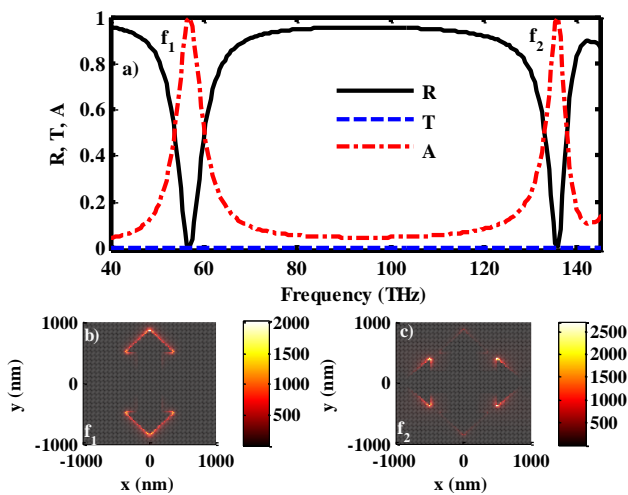
Fig. 2 (a) Spectral response of the PA with MgF_2 (b, c) Electric field distributions $|E|^2/|E_{int}|^2$ at (b) f_1 and (c) f_2 resonances

Figure 3(a) illustrates the A, R, and T spectra of the structure with SiO_2 dielectric spacer L = 1000nm, w_1 = 750 nm, w_2 = 700 nm, h_1 = 400 nm, h_2 =350 nm and d = 350 nm). Proposed PA has dual resonances and both of them rate as %99.8 at the first resonance

($f_1 = 58$ THz) and %99.9 at the second resonance ($f_2 = 132.5$ THz). Electric field distributions are given in Figs. 3(b) and 3(c) at first (f_1) and second (f_2) resonances, respectively. The near field enhancements are greater than 1500 times are concentrated on the sharp corners of the structure.
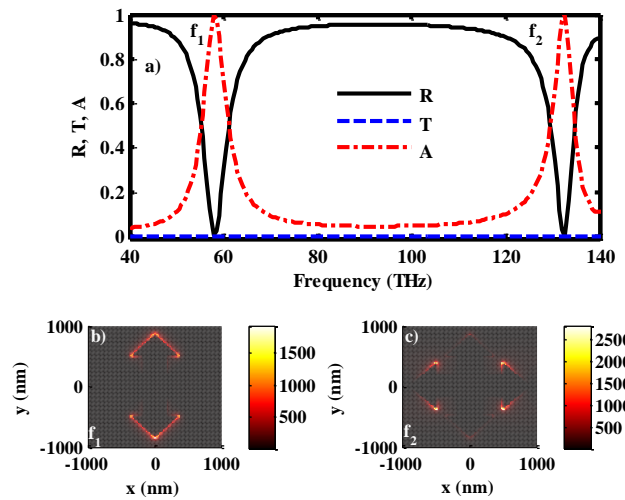
Fig. 3 (a) Spectral response of the PA with SiO_2 (b, c) Electric field distributions $|E|^2/|E_{int}|^2$ at (b) f_1 and (c) f_2 resonances.

In Fig. 4(a), the A, R, and T spectra of the structure with Al_2O_3 as dielectric spacer layer is given. Proposed PA has dual resonances and both of them rate as %98.4 at the first resonance ($f_1 = 51$ THz) and %99.8 at the second resonance ($f_2 = 118$ THz). Electric field distributions are given in Figs. 4(b) and 4(c) at first (f_1) and second (f_2) resonances, respectively. The near field enhancements are greater than 1500 times are concentrated on the sharp corners of the structure.
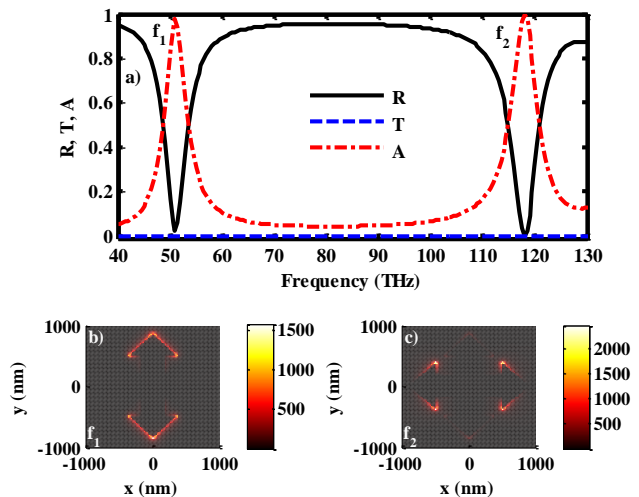

Fig. 4 (a) Spectral response of the PA with Al_2O_3 (b, c) Electric field distributions $|E|^2/|E_{int}|^2$ at (b) f_1 and (c) f_2 resonances.

Figure 5 demonstrates the changes in the spectral response for different d, L, h_1, h_2, w_1, w_2, and P parameter values. When the d (width of rectangular nanorods) increases, both of the resonance frequencies increase (Fig. 5a). Absorption spectra for L (length of rectangular nanorods) variation is given in Fig. 5b, which shows that both resonance frequencies of the structure decrease with the increasing length of rectangular nanorods, both of the resonance frequencies decrease. As the h_1 (heights of left and right triangular nanoparticles) increases, only second resonance frequency decreases slightly (Fig. 5c). When the h_2 (heights of

top and bottom triangular nanoparticles) increases, only first resonance frequency decreases (Fig. 5d). When the w_1 (base-widths of left and right triangular nanoparticles) increases, only second resonance frequency decreases (Fig. 5e) however only first resonance frequency decreases (Fig. 5f) with increasing w_2 (base-widths of the top and bottom triangular nanoparticles). The dependence of absorption spectra on the periodicity (P) is shown in Fig. 5g, which shows that only second resonance frequency is affected by the periodicity (P) variation. The optical characteristics of the proposed PA arrays are dependent on geometrical parameters (Fig. 5). The resonance frequencies of the proposed PA arrays can be tuned by changing the geometrical dimensions of PA arrays.
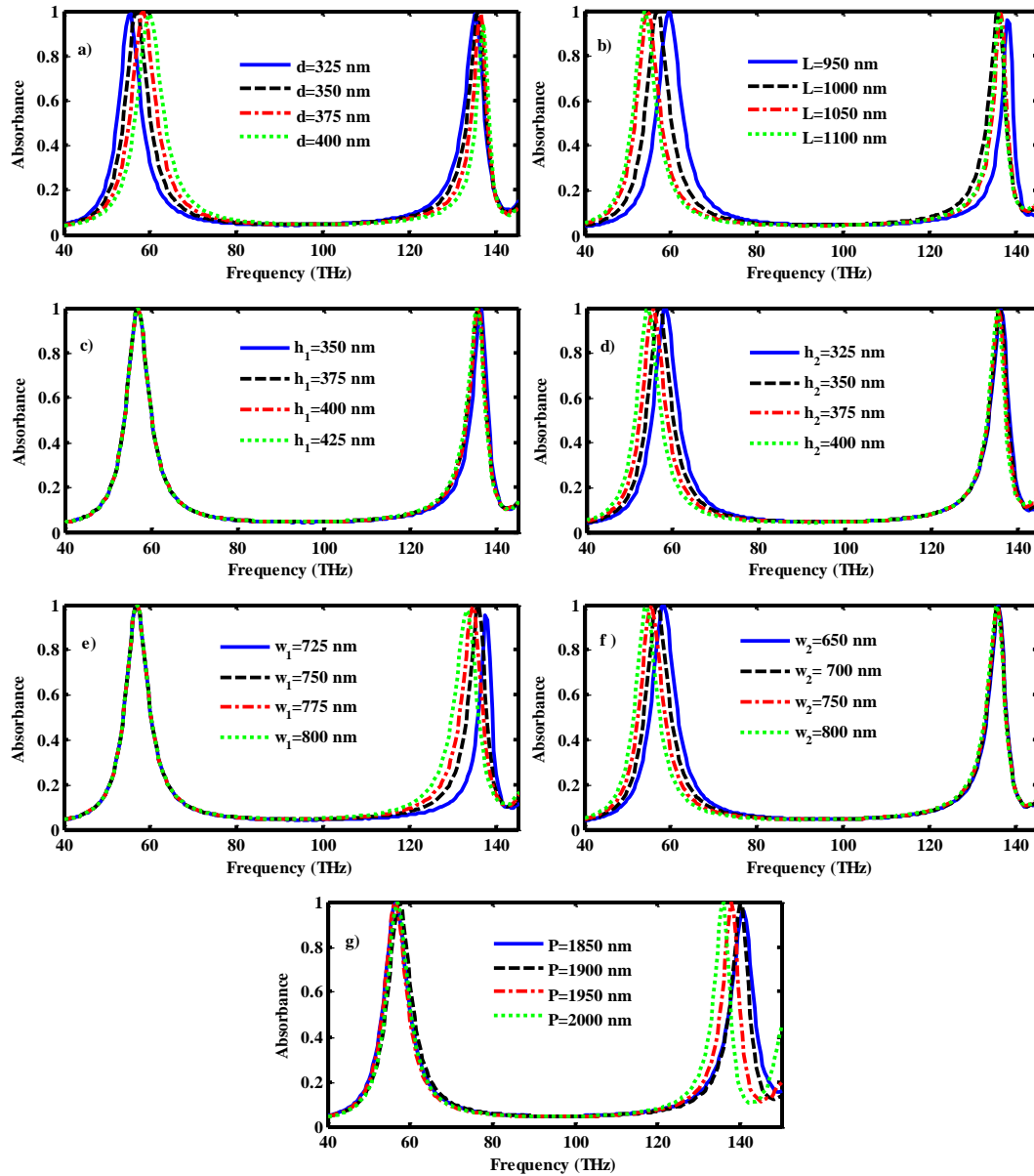

Fig. 5 Spectral response of proposed PAs (a) d variation and (b) L variation (c) h_1 variation (d) h_2 variation (e) w_1 variation (f) w_2 variation (g) P variation

In order to control the refractive index sensitivity of proposed PA array, the top of the structure is covered with cladding layers with different refractive indices (Fig. 6a). The cladding layer thicknesses are 100 nm. Linear correlation between the resonance frequencies and the refractive index of cladding mediums are determined. As the refractive index of the cladding medium increases, both of the resonance frequencies decrease (Fig. 6b).

3. Conclusion

In conclusion, a novel plasmonic PA array based on four-headed arrow nanoparticles for biosensing applications in mid-infrared regime is presented. The spectral response and near field distributions of the proposed PA array are obtained by using the FDTD method. The effects of the dielectric spacer on the spectral responses of the proposed PA array are determined. The highest absorption rates and near field enhancements are obtained PA array for MgF_2 dielectric spacer. Due to the dual-band spectral response and enhanced near-field distributions, the proposed dual-band four-headed arrow based PA array with adjustable spectral responses can be used for mid-infrared biosensing applications.
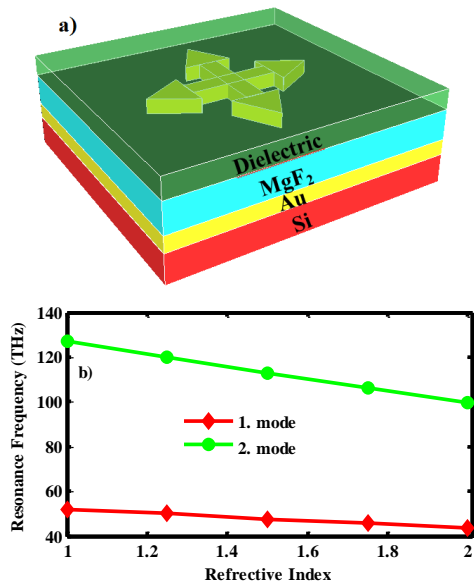
Fig. 6 (a) Schematic view of the proposed PA with cladding medium (b) Linear dependence between resonance frequencies and refractive indices

References

[1] Lubkowski G., Hirtenfelder F., Schuhmann R. and Weiland T. 3D full-wave field simulations of double negative metamaterial macrostructures, Proc. of Metamaterials, 2007, pp. 731–734.

[2] Liu N., Mesch M., Weiss T., Hentschel M. and Giessen H. Infrared perfect absorber and its application as plasmonic sensor, Nano Lett., Vol. 10, Number 7, 2010, pp. 2342-2348.

[3] Hedayati M. K., Javaherirahim M., Mozooni B., Abdelaziz R., Tavassolizadeh A., Chakravadhanula V. S. K., Zaporojtchenko V., Strunkus T., Faupel F. and Elbahri M. Design of a perfect black absorber at visible frequencies using plasmonic metamaterials, Adv Mater, Vol. 23, 2011, pp. 5410–5414.

[4] Fang Z., Zhen Y. R., Fan L., Zhu X. and Nordlander P. Tunablewideangle plasmonic perfect absorber at visible frequencies, Phys Rev B, Vol. 85, 2012, pp. 245401.

[5] Jamali A. A. and Witzigmann B. Plasmonic Perfect Absorbers for Biosensing Applications, Plasmonics, Vol.9, 2014, pp. 1265-1270.

[6] Hedayati M. K., Faupel F. and Elbahri M. Tunable broadband plasmonic perfect absorber at visible frequency, ApplPhys A, Vol. 109, 2014, pp. 769–773.

[7] Landy N. I., Sajuyigbe S., Mock J. J., Smith D. R. and Padilla W. J. Perfect metamaterial absorber, Phys Rev. Lett., Vol. 100, Number 207402, 2008, pp. 1–4.

[8] Wen Q. Y., Zhang H. W., Yang Q. H., Chen Z., Zhao B. H., Long Y. and Jing Y. L. Perfect metamaterial absorbers in microwave and terahertz bands, Metamaterial, 2012, pp. 501–512.

[9] Cattoni A., Ghenuche P., Gosnet A. M. H., Decanini D., Chen J., Pelouard J. L. and Collin S. λ3/1000 plasmonic nanocavities for biosensing fabricated by soft UV nanoimprint lithography, Nano Lett, Vol. 11, 2011, pp. 3557–3563.

[10] Diem M., Koschny T. and Soukoulis C. M. Wide-angle perfect absorber/thermal emitter in the terahertz regime, Phys Rev B, Vol. 79, 2009, pp. 033101-033104.

[11] LiG., ChenX., LiO., ShaoC., JiangY., HuangL., NiB., HuW. and LuW., A novel plasmonic resonance sensor based on an infrared perfect absorber, J. Phys. D: Appl. Phys., Vol. 45, 2012, pp. 205102.

[12] Zhang B., Zhao Y., Hao Q., Kiraly B., Khoo I. C., Chen S. and Huang T. J. Polarization-independent dual-band infrared perfect absorber based on a metal-dielectric-metal elliptical nanodisk array, Optics Express, Vol. 19, Number 16, 2011, pp. 15221- 15228.

[13] Chen K., Adato R. and Altug H. Dual-band perfect absorber for multispectral plasmon-enhanced infrared spectroscopy,ACS Nano, Vol. 6, Number 9, 2012, pp. 7998–8006.

[14] You J. B., Lee W. J., Won D. and Yu K., Multiband perfect absorbers using metal-dielectric films with optically dense medium for angle and polarization insensitive operation, Optics Express, Vol. 22, Number 7, 2014, pp. 8339- 8348.

[15] Cetin A. E., Korkmaz S., Durmaz H., Aslan E., Kaya S., Paiella R. and Turkmen M. Quantification of Multiple Molecular Fingerprints by Dual-Resonant Perfect Absorber, Advanced Optical Materials, 2016 (accepted).

[16] The numerical simulations are carried out using a finite-difference-time-domain package (Lumerical FDTD Solutions). [Online]. Available: www.lumerical.com

[17] Palik E.D. Handbook of Optical Constants of Solids, Academic, FL, 1985.